Research Square

Preprints are preliminary reports that have not undergone peer review.
They should not be considered conclusive, used to inform clinical practice,
or referenced by the media as validated information.

Spin-on phosphorus doping of planar and porous monocrystalline silicon with a solution derived from purified Tunisian natural phosphate: a feasibility comparison with POCl3 diffusion

Ridha Daik

ridhadaik@gmail.com

University of Hafr Al Batin

Sana Ben Amor

University of Hafr Al Batin

Hatem Ezzaouia

Research and Technology Center of Energy

Research Article

Keywords: Tunisian natural phosphate, spin-on doping, POCl3 diffusion, porous silicon, monocrystalline silicon, dark I–V, sheet resistance, minority-carrier lifetime

Posted Date: November 23rd, 2026

DOI: https://doi.org/10.21203/rs.3.rs-11684092/v1

License: This work is licensed under a Creative Commons Attribution 4.0 International License.
Read Full License

Additional Declarations: No competing interests reported.

Spin-on phosphorus doping of planar and porous monocrystalline silicon with a solution derived from purified Tunisian natural phosphate: a feasibility comparison with $POCl_3$ diffusion

Ridha Daik[1,3,*], Sana Ben Amor[2,3] and Hatem Ezzaouia[3]

[1] Preparatory Year, University of Hafr Al Batin, Saudi Arabia
[2] Department of Physics, College of Science, University of Hafr Al Batin, Saudi Arabia
[3] Research and Technology Center of Energy (CRTEn), Tunisia
* Corresponding author: ridhadaik@gmail.com

Abstract

In this work, p-type monocrystalline silicon was compared after phosphorus diffusion from two sources: commercial $POCl_3$ (Sidp) and a spin-on solution S extracted from purified Tunisian natural phosphate by nitric-acid dissolution and filtration. Solution S was applied on planar silicon (SidS) and on porous silicon (SipdS) formed by HF/HNO_3 vapour etching for 30 s, the etching time being selected by atomic force microscopy and reflectance. After diffusion at 925 °C for 45 min, hot-probe measurements showed n+ conduction in nearly all measurements on the three samples, and the sheet resistance of the doped layers was above that of the undoped control (107.23 Ω/sq). Dark I–V analysis, although strongly non-ideal, and effective minority-carrier lifetime measurements gave the same ranking: the best sample was porous silicon diffused with solution S (SipdS), which showed the lowest saturation current (0.92 µA against 10.34 µA for $POCl_3$), the lowest series resistance, the highest shunt resistance and the longest lifetime (92 µs against 31 µs). A phosphorus source derived from Tunisian phosphate therefore gives samples at least comparable to, and in this comparison better than, the $POCl_3$ reference; dopant profiles, passivated lifetime and device data are needed to confirm this.

Keywords: Tunisian natural phosphate; spin-on doping; $POCl_3$ diffusion; porous silicon; monocrystalline silicon; dark I–V; sheet resistance; minority-carrier lifetime

1. Introduction

The emitter is a decisive element of a crystalline silicon solar cell: its surface phosphorus concentration, depth profile and electrically inactive fraction control emitter recombination, contact formation and open-circuit voltage [1–3]. Tube-furnace diffusion from $POCl_3$ is the dominant industrial route [1,2], but it produces a heavily doped near-surface region in which phosphorus precipitates and becomes electrically inactive, increasing Shockley–Read–Hall recombination [4–7]; much recent work therefore aims to lower the surface concentration without losing contact quality [3,8–10]. Phosphorus diffusion is also a gettering step: the phosphosilicate glass (PSG) and the doped layer trap metallic impurities and raise the minority-carrier lifetime [11–15], a role exploited by the Tunisian groups together with a sacrificial porous silicon layer [16–18]. The same gettering concept was applied to the raw material of the present work, natural Tunisian phosphate [19,20].

Spin-on doping, in which a phosphorus-containing solution is spread by centrifugal force, dried and used as a solid source during the anneal, is a simple, low-cost and patternable alternative [21]. It is still investigated for selective emitters [22], passivating contacts [23,24], homojunction cells [25] and thin films [26], always with solutions formulated from commercial chemicals. Phosphoric acid, the usual phosphorus constituent of such solutions, is itself produced from phosphate rock; the question addressed here is whether purified natural phosphate, dissolved directly in nitric acid, can provide a usable dopant solution without the conventional acid-production chain. Tunisia has large sedimentary phosphate resources whose main phase is fluorapatite, $Ca_{10}(PO_4)_6F_2$, so such a route would add value to a local resource.

We also examine a porous silicon (PS) surface layer formed by HF/HNO_3 vapour etching [27], whose high surface area and graded refractive index have been used for antireflection, emitters and gettering [28–30] and which may influence the retention of the spin-on solution, although a lower reflectance does not always give

better cells [31]. The objectives are (i) to select the vapour-etching time that gives the most suitable porous layer, (ii) to form n^+ layers with solution S on planar and porous p-type silicon, and (iii) to compare their sheet resistance, conductivity type, dark electrical behaviour and effective minority-carrier lifetime with those of silicon diffused with commercial $POCl_3$.

2. Materials and methods

2.1 Experimental design

The study follows the sequence of Fig. 1. Porous layers made with exposure times of 0–40 s (E0–E40) were doped with solution S, and AFM and reflectance were used to select the etching time. The selected porous surface (E30, sample SipdS) and a planar surface (E0, sample SidS) were then compared with a planar surface doped with commercial $POCl_3$ (Sidp) by sheet resistance, hot-probe, dark I–V and lifetime measurements.

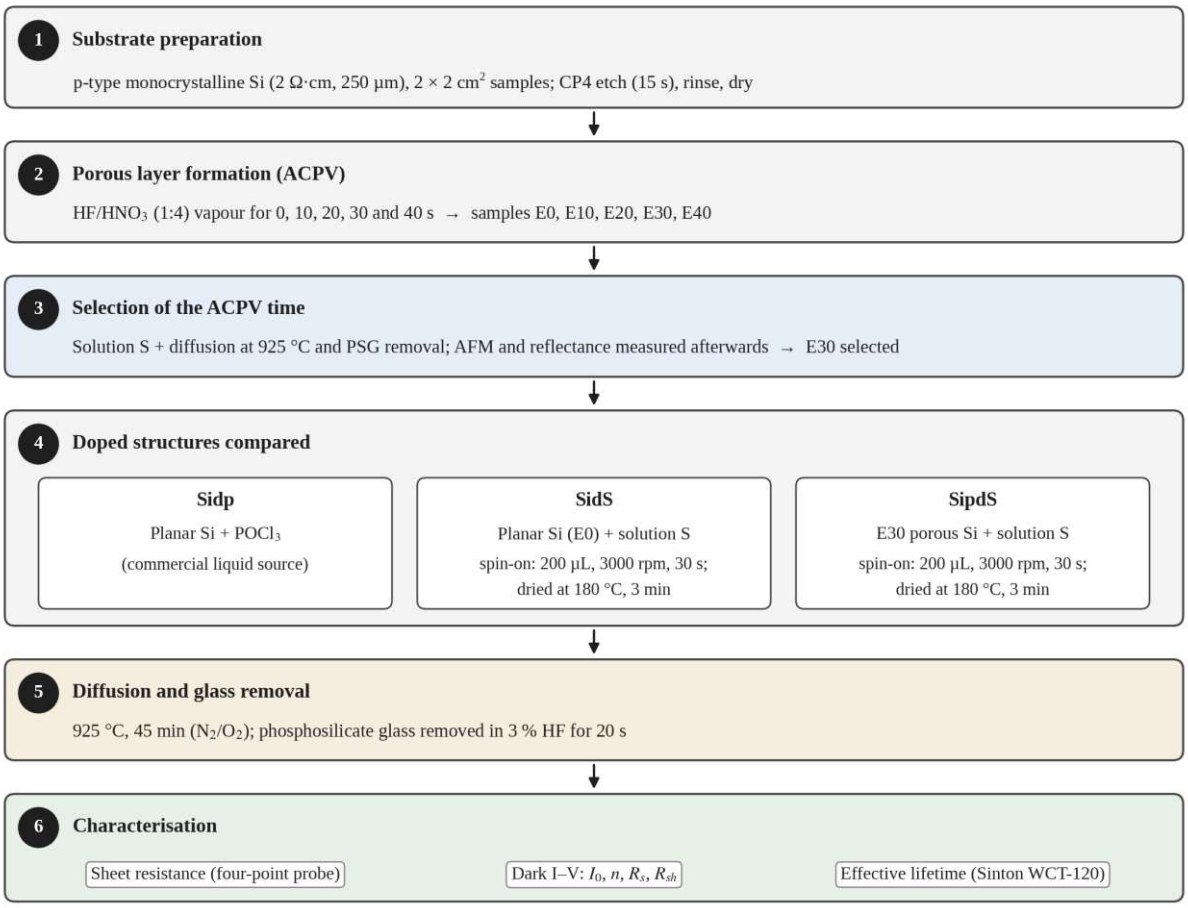


Fig. 1. Experimental flow: selection of the ACPV time by AFM and reflectance (measured after diffusion and PSG removal), doping with $POCl_3$ (Sidp) or with solution S (SidS, SipdS), diffusion, PSG removal and electrical characterisation.

2.2 Substrates and porous layer formation

P-type monocrystalline silicon wafers (250 µm thick, 2 Ω·cm) were cut into 2 × 2 cm^2 samples, etched for 15 s in an $HF/HNO_3/CH_3COOH$ solution (CP4-type, 1:3:5), rinsed in deionised water for 90 s and dried at 85 °C for 30 min. Porous layers were formed by acid chemical vapour etching (ACPV) [27]: the samples were exposed for 10, 20, 30 or 40 s to the vapour of an HF/HNO_3 (1:4) solution, held 10 cm above the liquid surface at 25 °C in a 20 mL container, and are named E10–E40 (E0: no exposure). In the vapour, nitric acid oxidises silicon and HF dissolves the oxide formed.

2.3 Dopant sources

$POCl_3$ reference (Sidp). A planar silicon sample was diffused in a conventional tube furnace at 925 °C for 45 min under oxygen with commercial $POCl_3$, used as received.

Phosphate-derived solution (S). The Tunisian natural phosphate was first purified by a gettering treatment [19,20]. The purified phosphate (R4) was dispersed at 5 mg mL^{-1} in nitric acid and stirred for 1 h at pH 2, where the fluorapatite dissolves ($Ca_{10}(PO_4)_6F_2 + 12\ H^+ \rightarrow 10\ Ca^{2+} + 6\ H_2PO_4^- + 2\ F^-$). The suspension was filtered, and the filtrate was heated at 60 °C for 2 h to concentrate the phosphorus species and mixed with butanol and acetone (1:1, v/v) to give solution S (Fig. 2). ICP-OES showed that S is rich in phosphorus and that the purification of the phosphate reached 99.996 % [20].

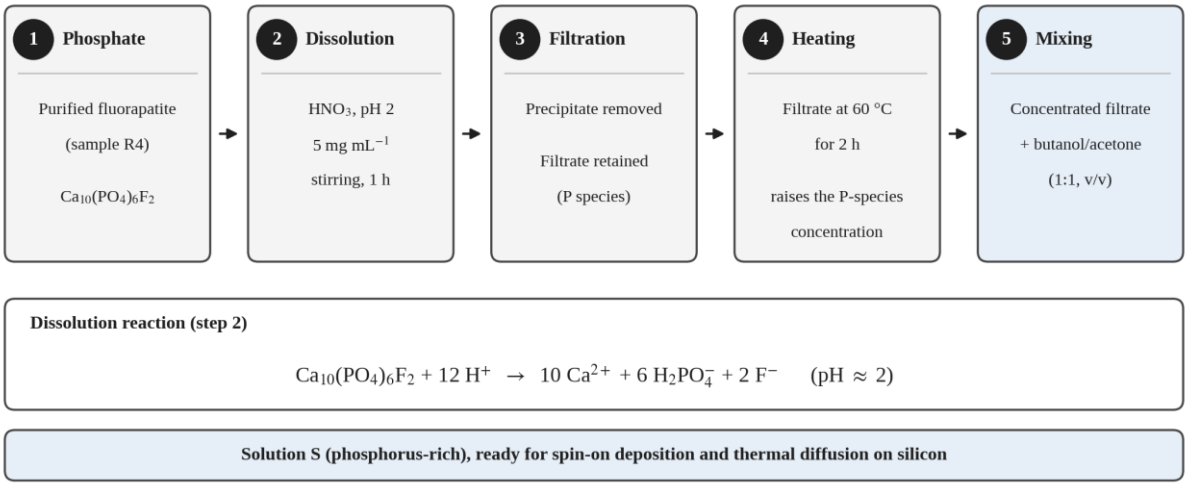


Fig. 2. Preparation of the spin-on doping solution S: (1) purified phosphate R4; (2) dissolution in nitric acid under stirring (5 mg mL^{-1}, pH 2, 1 h); (3) filtration, the precipitate being removed; (4) heating of the filtrate at 60 °C for 2 h; (5) mixing with butanol and acetone (1:1, v/v) to give solution S, ready for diffusion.

2.4 Spin-on deposition, diffusion and glass removal

Solution S (200 µL) was spun at 3000 rpm for 30 s on each sample and dried on a hot plate at 180 °C for 3 min. SidS (planar silicon, E0) and SipdS (E30 porous silicon, formed first and doped with S afterwards) were annealed at 925 °C for 45 min in an infrared-lamp furnace under N_2/O_2, and the PSG was removed in 3 % HF for 20 s. All samples were diffused under the same nominal temperature and time, so the comparison reflects the dopant source and the surface preparation.

2.5 Characterisation

Surface topography and RMS roughness (Rq) were obtained by contact-mode atomic force microscopy (Digital Instruments NanoScope multimode) over 5 × 5 µm² (512 × 512 points, 1 Hz). Reflectance spectra were recorded after PSG removal between 200 and 2500 nm with a PerkinElmer Lambda 950 spectrophotometer with an integrating sphere. Sheet resistance was measured with a Jandel RM3000+ four-point probe in a nine-point configuration, on the doped samples and on an undoped control. The conductivity type was checked by the hot-probe method with the probe at 45 °C; four measurements were made on each sample and the mean hot-probe voltage was recorded. Dark I–V curves were recorded at room temperature with a Keithley 2400 source-measure unit between aluminium contacts on the two opposite faces of the 2 × 2 cm^2 samples (two-terminal, through-plane; contacted area about 2 mm²; −5 to +5 V in 0.05 V steps), so that the extracted resistances include the substrate and the Al–silicon contacts. For the 250 µm, 2 Ω·cm substrate the calculated sheet resistance is $\rho/t \approx 80$ Ω/sq. Effective minority-carrier lifetimes were measured on the diffused, unpassivated samples (PSG removed) with a Sinton WCT-120 photoconductance system [32] at $\Delta n = 5 \times 10^{14}$ cm^{-3} in generalised mode (optical constant 0.7), repeated four times at 5 min intervals to check stability; the lifetime is an effective value combining bulk, surface and emitter recombination. Several samples were prepared and measured for each condition, and the values reported are condition-level averages.

2.6 Analysis of the dark I–V data

The dark current was described by the single-diode relation (Eqs. 1 and 2), the ideality factor n being obtained from the slope of ln I versus V, and by a model including series (R_s) and shunt (R_{sh}) resistances (Eq. 3). Because n is defined locally and a single value depends on the fitted voltage window, the local form (Eq. 4) was used as a diagnostic [33].

$$I = I_0[\exp(qV/nkT) - 1] \quad (1)$$

$$\ln I = \ln I_0 + qV/nkT \quad (2)$$

$$I = I_0[\exp(q(V - R_sI)/nkT) - 1] + (V - R_sI)/R_{sh} \quad (3)$$

$$n(V) = (q/kT)\cdot(\mathrm{d}\ln I/\mathrm{d}V)^{-1} \quad (4)$$

3. Results and discussion

3.1 Selection of the ACPV time: AFM and reflectance

Fig. 3 shows the AFM images of E0–E40. The unetched surface E0 is granular (Rq = 2.50 nm); Rq rises to 8.00 nm at 10 s and 17.7 nm at 20 s and reaches its maximum of 34.4 nm at 30 s (13.7 times E0), where a regular array of closely spaced round features covers the whole scan, and then falls to 10.7 nm at 40 s. This suggests growth of the porous layer up to about 30 s followed by a partial loss or merging of the tallest features at longer exposure; the behaviour beyond 40 s was not examined.

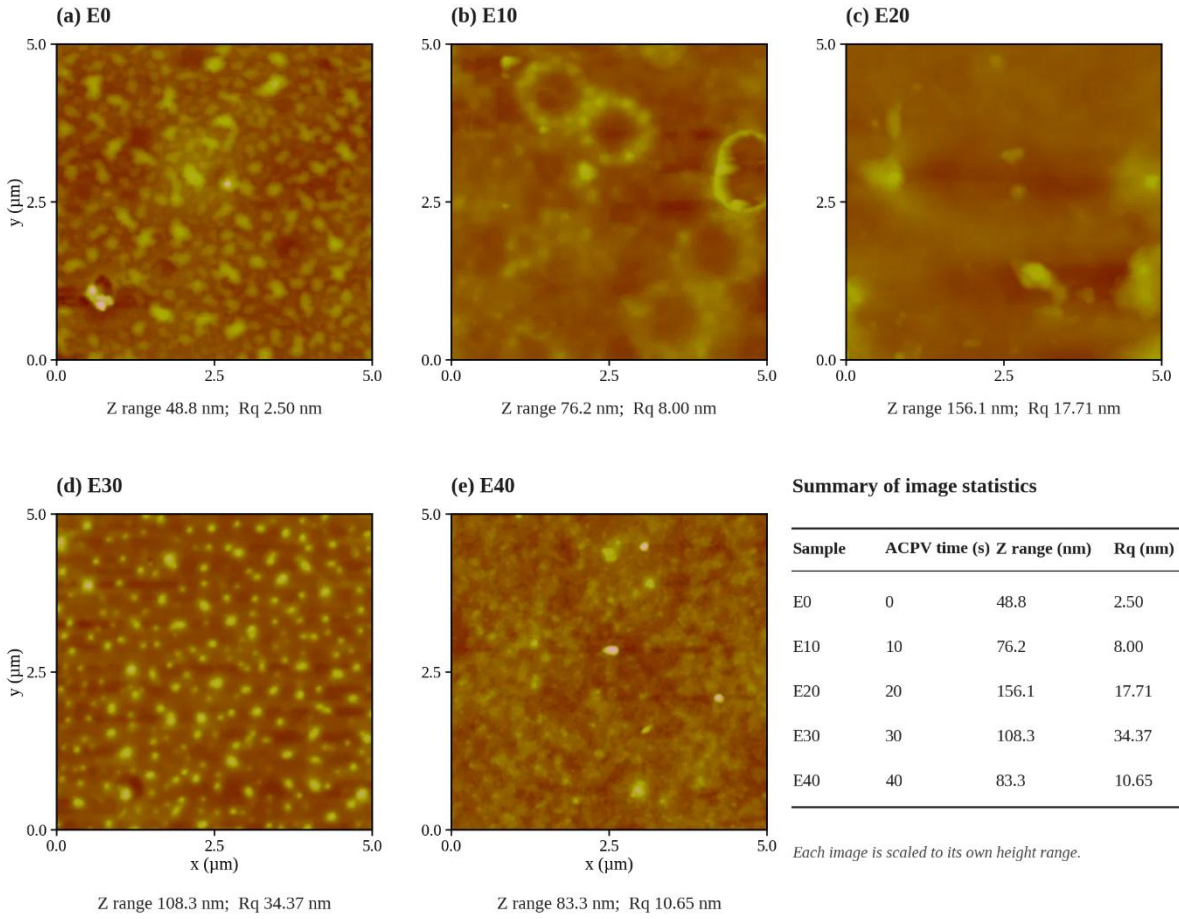


Fig. 3. AFM images (5 × 5 µm²) of the silicon surface after ACPV exposure for 0 (E0), 10 (E10), 20 (E20), 30 (E30) and 40 s (E40); the Z range and the RMS roughness (Rq) of each image are given below the panels.

The reflectance spectra (Fig. 4) show the usual silicon behaviour, with a plateau between about 500 and 900 nm where the order is E0 (highest) > E40 ≈ E10 > E20 ≳ E30 (lowest). E0 is at about 28–29 % and E30 at about 23–24 %, a reduction of about 5 percentage points (about 18 % relative), most plausibly caused by the

graded effective refractive index and the scattering of the porous surface [28–30]. All spectra were measured after diffusion and PSG removal and E0 received the same diffusion, so the difference is attributed to the porous layer, although changes in the doped layer cannot be excluded because an undiffused porous control was not measured. The reduction is modest compared with alkaline texturing or an antireflection coating, and a lower reflectance should not be read as a device-level benefit [31].

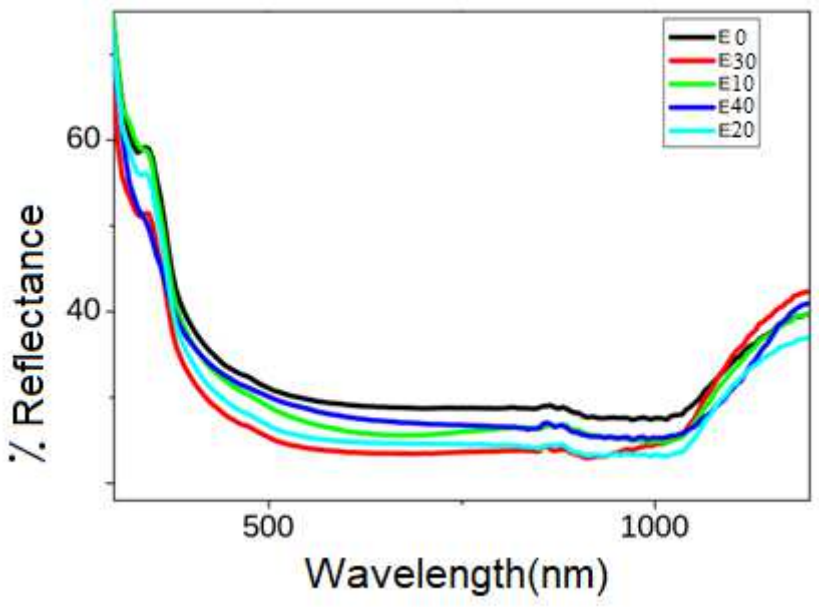


Fig. 4. Reflectance spectra, measured after diffusion with solution S and PSG removal, of the silicon samples prepared with different ACPV times (E0, E10, E20, E30, E40), shown between about 300 and 1200 nm.

Together, AFM and reflectance identify 30 s as the most suitable ACPV time (largest roughness, lowest reflectance), and E30 was retained for SipdS. RMS roughness depends on scan size and tip geometry and does not give the thickness or porosity of the layer, so the data identify a favourable etching time and not the structure of the porous layer.

3.2 Sheet resistance and conductivity type

Table 1 gives the sheet resistance after PSG removal and the hot-probe results. The undoped control gave 107.23 Ω/sq, somewhat above the 80 Ω/sq calculated for the substrate. All doped samples are above it: Sidp ($POCl_3$) 124.4 Ω/sq (1.16 times), SidS 207.3 Ω/sq (1.93 times) and SipdS 361.23 Ω/sq (3.37 times), as expected when the probe current is confined to a layer separated from the p-type substrate by a junction; the Sidp value, only 16 % above the control, is however weak evidence on its own. The hot-probe measurements, in which nearly all points indicated n+ conduction, confirm the formation of an n-type layer on all three samples, but they identify the conductivity type only and are not a measure of the dose. The higher sheet resistance of SipdS suggests a lower effective dose, poorer dopant incorporation or a different current path in the porous structure. Sidp lies just above the 60–120 Ω/sq range targeted for lightly doped industrial emitters [3,22], and SidS and SipdS correspond to a lower active dose. These emitters are proofs of concept and not optimised ones: the junction depth, dose and inactive phosphorus [4,5,34] can only be settled by ECV or SIMS profiles, and a dilution series or a drive-in step should be examined [3,10].

Table 1. Sheet resistance after PSG removal and hot-probe results (probe at 45 °C, mean of four measurements).

Sample	Sheet resistance (Ω/sq)	Hot-probe mean voltage (mV)	Type
Undoped control	107.23	—	—
Sidp ($POCl_3$)	124.4	9.53	n^+
SidS (S, planar)	207.3	6.21	n^+
SipdS (S, E30)	361.23	1.80	n^+

3.3 Dark current–voltage characteristics

Fig. 5 compares the dark I–V curves of Sidp, SidS and SipdS. All curves are asymmetric but far from good rectification: forward and reverse currents are of the same order (about 1 mA) for |V| < 1.5 V and the reverse current keeps rising with |V|, as for a leakage path. The forward-to-reverse current ratio at ±0.4 V is about 0.7 for Sidp, 2 for SidS and 5 or more for SipdS (values read by eye), so the $POCl_3$ sample hardly rectifies and the phosphate-derived samples, especially the porous one, rectify better. The poor rectification of Sidp points to contacts, probing geometry or edge and rear-side leakage governing these curves, so the differences between samples reflect the whole measurement structure and not only the dopant chemistry.

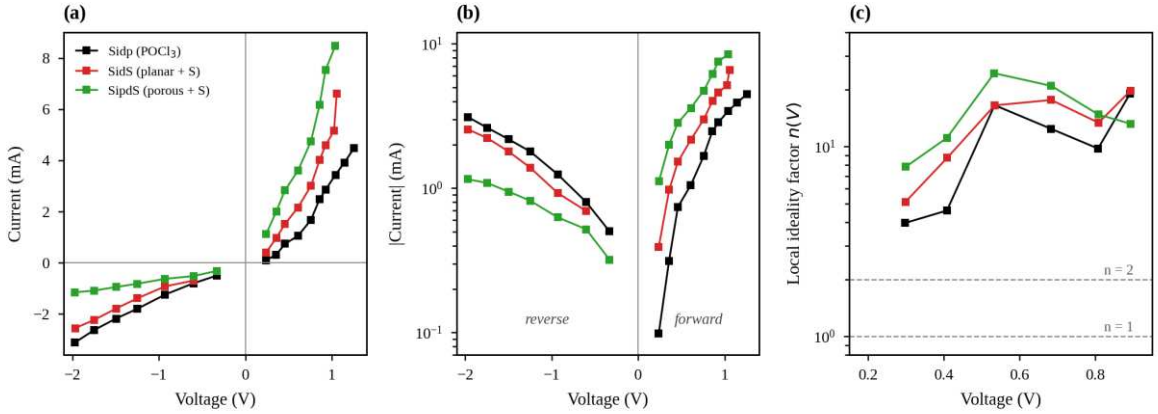


Fig. 5. Dark I–V characteristics of Sidp ($POCl_3$), SidS (planar Si + S) and SipdS (E30 porous Si + S): (a) current versus voltage; (b) absolute current on a logarithmic scale for both polarities; (c) local ideality factor n(V) of the forward branch. Data re-plotted from the measured curves.

Table 2 gives the parameters of the single-diode fit. The phosphate-derived samples show a saturation current 10–11 times lower than Sidp (0.98 and 0.92 µA against 10.34 µA), a 2.5–3.5 times lower series resistance and a 1.5–2.1 times higher shunt resistance, so I_0, R_s and R_{sh} all change in the favourable direction, most for SipdS. The ideality factors of 3.1–4.2 (3.3–3.7 reported for spin-on-doped cells [35]) and the local n(V) of Fig. 5c, which is not constant and exceeds 10 above 0.4–0.5 V, show that the curves cannot be interpreted as a single p–n junction: trap-assisted tunnelling, shunts and non-uniform contact resistance are typical causes [36–39], and a two-diode model describes such curves better [33,37]. The lower apparent n of the S-doped samples is therefore not significant, I_0 and n are correlated in a one-diode fit, and R_{sh} of 61–130 Ω (about 250–520 Ω·cm^2 for the full 4 cm^2 area) indicates a leaky structure. These parameters indicate feasibility and not a ranking of the two sources.

Table 2. Parameters from the single-diode fit of the dark I–V curves.

Sample	I_0 (µA)	n	R_s (Ω)	R_{sh} (Ω)
Sidp	10.34	4.2	23.61	61.47
SidS	0.98	3.6	9.43	89.31
SipdS	0.92	3.1	6.68	130.32

3.4 Effective minority-carrier lifetime

The effective minority-carrier lifetime (τ_{eff}) combines recombination in the bulk and at the surfaces of the wafer. Assuming uniform carrier generation in the silicon wafer, it can be written as [40]:

$$\frac{1}{\tau_{eff}} \approx \frac{1}{\tau_b} + \frac{2S_{eff}}{W} \quad (5)$$

where τ_b is the bulk lifetime, S_{eff} the effective surface recombination velocity and W the wafer thickness. As the surfaces carry a phosphorus-diffused region and no passivation, S_{eff} lumps together surface and emitter recombination, and τ_b reflects the bulk impurity content, which phosphorus diffusion and porous-silicon gettering are expected to modify [16,17].

Fig. 6 shows τ_{eff} at $\Delta n = 5 \times 10^{14}$ cm^{-3}: about 31 µs for Sidp, 61 µs for SidS and 92 µs for SipdS, stable within about 1 µs over the four measurements. The S-doped samples therefore show an effective lifetime about 2 times (SidS) and 3 times (SipdS) that of the $POCl_3$ reference, and the porous sample is about 50 % above its planar counterpart.

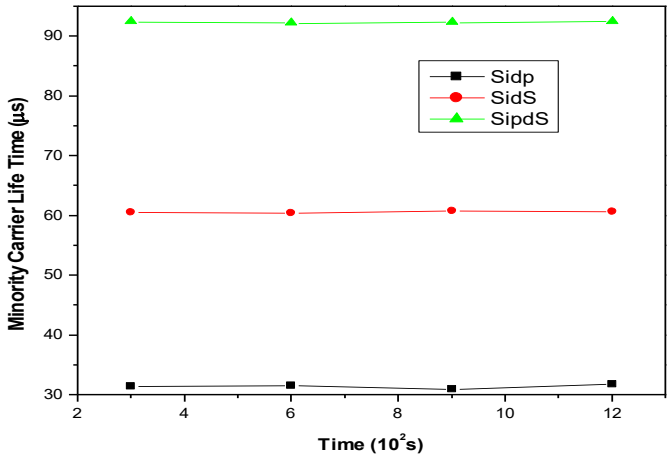


Fig. 6. Effective minority-carrier lifetime of Sidp ($POCl_3$), SidS (planar Si + S) and SipdS (E30 porous Si + S), measured with a Sinton WCT-120 at $\Delta n = 5 \times 10^{14}$ cm^{-3}; the measurement was repeated every 5 min.

Being contactless, this measurement is not affected by the contact and edge problems of the dark I–V data, so the order Sidp < SidS < SipdS is not a contacting artefact. It is compatible with gettering by the PSG and by the porous layer [14,16–18], the highest lifetime being obtained for the sample that combines solution S with the porous surface, but other explanations give the same order: a lower surface or emitter recombination (τ_{eff} increases in the same order as the sheet resistance, as expected if a lower active dose reduced the emitter recombination) or a different thermal history. A single-injection measurement on unpassivated samples cannot discriminate between them [40], and no extended low-temperature hold of the kind used by Kim et al. [14] was applied here, so a bulk-gettering contribution cannot be assumed from a single 45 min anneal. The lifetime data therefore show only that the use of solution S is not accompanied by a lower effective lifetime than $POCl_3$; they do not demonstrate gettering or passivation.

3.5 Comparison with $POCl_3$ and related work

Taken together, the measurements give a coherent picture: the ACPV treatment has an optimum near 30 s, the optimum sample has the lowest reflectance, and the combination of the porous surface with solution S gives the lowest fitted I_0, R_s and apparent n, the highest R_{sh} and the highest effective lifetime of the three samples, so SipdS is the best sample measured here. The origin of these differences cannot be assigned with the present data. Solution S is derived from fluorapatite and may carry calcium, fluoride and trace metals into the PSG and the silicon; ICP-OES shows that the trace metals were removed in the purification step [20], but residual contamination of the silicon should still be checked directly, since impurities introduced by the diffusion are not always removed by cleaning [13]. This is the central question for a phosphate-derived dopant, and the present data address it only indirectly.

Table 3. Selected related studies on phosphorus emitter formation and phosphorus-diffusion gettering.

Study	Phosphorus source / process	Structure	Reported outcome
Fangsuwannarak et al. 2019 [22]	TEOS:H_3PO_4 spin-on solution; 1000 °C, 30 min	n^+ selective emitter on Si	Emitter regions of 35 and 121 Ω/sq formed in one step
Mohamad et al. 2024 [25]	Spin-on doping, 1–8 layers	p-type Si homojunction cell	Efficiency improved from 1 to 4 layers; 6 and 8 layers degraded R_s and R_{sh}
Xu et al. 2023 [3]	$POCl_3$, three-step low–high–low process	p-type multicrystalline Si cells	≈ 90 Ω/sq; lower surface concentration; +1 mV V_{oc}, +0.3 % FF, +0.1 % efficiency
Ali et al. 2012 [35]	Spin-on phosphorus source (P8545SF), 900–1100 °C, 60 min	p-type Si (1 Ω·cm), n^+ emitter, dark I–V	Sheet resistance 108 to 10 Ω/sq (900–1100 °C); n = 3.3–3.7; best at 950 °C (40 Ω/sq)
Derbali and Ezzaouia 2012 [17]	$POCl_3$ diffusion into a sacrificial PS layer	mc-Si, gettered	Improved R_s, R_{sh} and photovoltaic parameters from dark I–V and IQE
Kim et al. 2013 [14]	Phosphorus diffusion at 850 °C, then 700 °C for 5 h	Single-crystalline, multi-crystalline and UMG Si wafers	Higher minority-carrier lifetime after gettering (QSSPC and μW-PCD)
This work	Solution S from purified Tunisian phosphate vs $POCl_3$; 925 °C, 45 min	p-type mono-Si, planar or porous	124.4–361.23 Ω/sq, n^+ by hot probe; dark I–V and τ_{eff} (≈ 31–92 μs); no profile or device data

Table 3 shows that spin-on phosphorus sources can reach device-grade quality when the dose, the thermal budget and the passivation are controlled [23–25], and that the emitter must be engineered for low surface concentration [3,7]. The distinctive element of the present work is the origin of the phosphorus and its direct comparison with the industrial $POCl_3$ route on the same substrate type; the quantities measured in those studies (dopant profile, passivated injection-dependent lifetime, implied V_{oc}, contact resistivity, efficiency) remain to be measured here.

4. Limitations and outlook

The dopant profile, junction depth and active carrier density were not measured, the dark I–V parameters are strongly non-ideal and the lifetimes come from unpassivated samples, so the results indicate feasibility and not a firm ranking, and no illuminated device data are available. Future work should add dopant profiling, a dose series, passivated lifetime and illuminated cell measurements.

5. Conclusions

AFM and reflectance identified 30 s as the most suitable vapour-etching time (largest roughness, 34.4 nm; lowest reflectance, about 5 percentage points below the unetched surface). Silicon diffused at 925 °C for 45 min with commercial $POCl_3$ or with a spin-on solution extracted from purified Tunisian natural phosphate showed n+ conduction by hot probe, with sheet resistances above that of the undoped control. In the dark, the phosphate-derived samples showed a lower fitted saturation current and series resistance and a higher shunt resistance than the $POCl_3$ sample, and a higher effective minority-carrier lifetime (up to 92 μs against 31 μs); the best sample was porous silicon diffused with solution S (SipdS). Because all samples are strongly non-ideal and unpassivated, the work is a feasibility demonstration: the phosphate-derived source is at least comparable to $POCl_3$ and gave better results in this comparison, but dopant profiles, passivated lifetime and illuminated device data are needed before superiority can be claimed.

Declarations

CRediT authorship contribution statement. Ridha Daik: Conceptualization, Methodology, Investigation, Formal analysis, Writing – original draft. Sana Ben Amor: Investigation, Writing – review & editing. Hatem Ezzaouia: Supervision, Writing – review & editing.

Declaration of competing interest. The authors declare that they have no known competing financial interests or personal relationships that could have appeared to influence the work reported in this paper.

Declaration of generative AI and AI-assisted technologies in the writing process. During the preparation of this work the authors used Claude (Anthropic) to improve language, structure and formatting. After using this tool, the authors reviewed and edited the content as needed and take full responsibility for the content of the publication.

Funding. This research did not receive any specific grant from funding agencies in the public, commercial, or not-for-profit sectors.

Data availability. The data that support the findings of this study are available from the corresponding author on reasonable request.

References

[1] H. Li, K. Kim, B. Hallam, B. Hoex, S. Wenham, M. Abbott, $POCl_3$ diffusion for industrial Si solar cell emitter formation, *Front. Energy* 11 (2017) 42–51. https://doi.org/10.1007/s11708-016-0433-7

[2] A. Wolf, A. Kimmerle, S. Werner, S. Maier, U. Belledin, S. Meier, D. Biro, Status and perspective of emitter formation by $POCl_3$-diffusion, *Proc. 31st European Photovoltaic Solar Energy Conference*, Hamburg, 2015, pp. 414–419.

[3] X. Xu, W. Wu, Q. Wang, Efficiency improvement of industrial silicon solar cells by the $POCl_3$ diffusion process, *Materials* 16 (2023) 1824. https://doi.org/10.3390/ma16051824

[4] B. Min, H. Wagner, A. Dastgheib-Shirazi, A. Kimmerle, H. Kurz, P. P. Altermatt, Heavily doped Si:P emitters of crystalline Si solar cells: recombination due to phosphorus precipitation, *Phys. Status Solidi RRL* 8 (2014) 680–684. https://doi.org/10.1002/pssr.201409138

[5] A. Dastgheib-Shirazi, M. Steyer, G. Micard, H. Wagner, P. P. Altermatt, G. Hahn, Relationships between diffusion parameters and phosphorus precipitation during the $POCl_3$ diffusion process, *Energy Procedia* 38 (2013) 254–262. https://doi.org/10.1016/j.egypro.2013.07.275

[6] M. Steyer, A. Dastgheib-Shirazi, G. Hahn, B. Terheiden, New method for determination of electrically inactive phosphorus in n-type emitters, *Energy Procedia* 77 (2015) 316–320. https://doi.org/10.1016/j.egypro.2015.07.045

[7] H. Wagner, A. Dastgheib-Shirazi, B. Min, A. E. Morishige, M. Steyer, G. Hahn, C. del Cañizo, T. Buonassisi, P. P. Altermatt, Optimizing phosphorus diffusion for photovoltaic applications: peak doping, inactive phosphorus, gettering, and contact formation, *J. Appl. Phys.* 119 (2016) 185704. https://doi.org/10.1063/1.4949326

[8] H. J. Lee, M. G. Kang, S. J. Choi, G. H. Kang, J. M. Myoung, H. E. Song, Characteristics of silicon solar cell emitter with a reduced diffused phosphorus inactive layer, *Curr. Appl. Phys*. 13 (2013) 1718–1722. https://doi.org/10.1016/j.cap.2013.06.020

[9] H. Li, F.-J. Ma, Z. Hameiri, S. Wenham, M. Abbott, On elimination of inactive phosphorus in industrial $POCl_3$ diffused emitters for high efficiency silicon solar cells, *Sol. Energy Mater. Sol. Cells* 171 (2017) 213–221. https://doi.org/10.1016/j.solmat.2017.06.040

[10] K. Panchal, P. Zala, U. Kumar, M. Bhaisare, C. M. Kumar, I. Mukhopadhyay, A. Ray, Conformity of multi-step diffusion optimization towards high efficiency industrial mono-PERC Si-solar cells, *Next Mater.* **9** (2025) 101249. https://doi.org/10.1016/j.nxmate.2025.101249

[11] A. Bentzen, A. Holt, Overview of phosphorus diffusion and gettering in multicrystalline silicon, *Mater. Sci. Eng. B* 159–160 (2009) 228–234. https://doi.org/10.1016/j.mseb.2008.10.060

[12] E. Cho, Y.-W. Ok, L. Dahal, A. Das, V. Upadhyaya, A. Rohatgi, Comparison of $POCl_3$ diffusion and phosphorus-ion-implantation induced gettering in crystalline Si solar cells, *Sol. Energy Mater. Sol.* Cells 157 (2016) 245–249.

[13] D. X. Du et al., Revealing the effect of phosphorus diffusion gettering on industrial silicon heterojunction solar cell, *Sol. Energy Mater. Sol. Cells* 282 (2025) 113392. https://doi.org/10.1016/j.solmat.2024.113392

[14] J. Kim, S. Y. Yoon, K. Choi, Effects of phosphorus diffusion gettering on minority carrier lifetimes of single-crystalline, multi-crystalline and UMG silicon wafer, *Curr. Appl. Phys.* 13 (2013) 2103–2108. https://doi.org/10.1016/j.cap.2013.09.013

[15] T. Jiang, X. Yu, R. Fan, X. Gu, D. Yang, Phosphorus diffusion gettering of substitutional metal contaminants at a small-angle grain boundary in n-type silicon: the case of gold, *J. Cryst. Growth* 380 (2013) 51–54. https://doi.org/10.1016/j.jcrysgro.2013.05.034

[16] N. Khedher, M. Hajji, M. Hassen, A. BenJaballah, B. Ouertani, H. Ezzaouia, B. Bessais, A. Selmi, R. Bennaceur, Gettering impurities from crystalline silicon by phosphorus diffusion using a porous silicon layer, *Sol. Energy Mater. Sol. Cells* 87 (2005) 605–611. https://doi.org/10.1016/j.solmat.2004.09.017

[17] L. Derbali, H. Ezzaouia, Phosphorus diffusion gettering process of multicrystalline silicon using a sacrificial porous silicon layer, *Nanoscale Res. Lett. 7* (2012) 424. https://doi.org/10.1186/1556-276X-7-424

[18] L. Derbali, A. Zarroug, H. Ezzaouia, Minority carrier lifetime and efficiency improvement of multicrystalline silicon solar cells by two-step process, *Renew. Energy* 77 (2015) 331–337.

[19] R. Daik, M. Lajnef, S. Ben Amor, S. Elgharbi, H. Meddeb, K. Abdessalem, M. Férid, H. Ezzaouia, Application of gettering process on the improvement of the structural and mineralogical properties of Tunisian phosphate rock, *J. Mater. Sci. Eng.* 5 (2016) 222. https://doi.org/10.4172/2169-0022.1000222

[20] R. Daik, M. Lajnef, S. Ben Amor, H. Ezzaouia, Effect of the temperature and the porosity of the gettering process on the removal of heavy metals from Tunisian phosphate rock, *Results Phys.* 7 (2017) 4189–4194.

[21] B. Hartiti, A. Slaoui, J. C. Muller, R. Stuck, P. Siffert, Phosphorus diffusion into silicon from a spin-on source using rapid thermal processing, *J. Appl. Phys.* 71 (1992) 5474–5478.

[22] T. Fangsuwannarak, S. Laohawiroj, K. Mekmork, Synthesis of phosphorus solution for n^+ Si selective emitter solar cell by spin on doping, *E3S Web Conf.* 122 (2019) 02006. https://doi.org/10.1051/e3sconf/201912202006

[23] Z. Ding, D. Yan, J. Stuckelberger, S. P. Phang, W. Chen, C. Samundsett, J. Yang, Z. Wang, P. Zheng, X. Zhang, Y. Wan, D. Macdonald, Phosphorus-doped polycrystalline silicon passivating contacts via spin-on doping, *Sol. Energy Mater. Sol. Cells* 221 (2021) 110902.

[24] J. Ibarra Michel, D. Yan, S. P. Phang, T. Zheng, B. C. Johnson, J. Yang, X. Zhang, W. Chen, Y. Wan, T. Truong, J. Stuckelberger, Y. Pan, D. Macdonald, J. Bullock, Poly-Si passivating contacts prepared via phosphorus spin-on-doping: a comparison between different silicon deposition methods, *Sol. Energy Mater. Sol. Cells* 255 (2023) 112290. https://doi.org/10.1016/j.solmat.2023.112290

[25] I. S. Mohamad, P. J. Ker, P. Chelvanathan, M. N. Norizan, B. K. Yap, S. K. Tiong, N. Amin, An experimental investigation of spin-on doping optimization for enhanced electrical characteristics in silicon homojunction solar cells: proof of concept, *Heliyon* 10 (2024) e31193. https://doi.org/10.1016/j.heliyon.2024.e31193

[26] C. Barri, E. Mafakheri, L. Fagiani, G. Tavani, A. Barzaghi, D. Chrastina, A. Fedorov, J. Frigerio, M. Lodari, F. Scotognella, E. Arduca, M. Abbarchi, M. Perego, M. Bollani, Engineering of the spin on dopant process on silicon on insulator substrate, *Nanotechnology* 32 (2021) 025303.

[27] M. Saadoun, N. Mliki, H. Kaabi, K. Daoudi, B. Bessaïs, H. Ezzaouia, R. Bennaceur, Vapour-etching-based porous silicon: a new approach, *Thin Solid Films 405* (2002) 29–34.

[28] R. R. Bilyalov, R. Lüdemann, W. Wettling, L. Stalmans, J. Poortmans, J. Nijs et al., Multicrystalline silicon solar cells with porous silicon emitter, *Sol. Energy Mater. Sol. Cells 60* (2000) 391–420.

[29] A.-M. Mouafki et al., Porous silicon antireflective coatings for silicon solar cells, *Eng. Technol. Appl. Sci. Res. 12* (2022) 8354–8358.

[30] A. Zarroug, W. Dimassi, R. Ouertani, H. Ezzaouia, Mechanical grooving of oxidized porous silicon to reduce the reflectivity of monocrystalline silicon solar cells, *Phys. Status Solidi* C 9 (2012) 2128–2130. https://doi.org/10.1002/pssc.201200257.

[31] N. Marrero, R. Guerrero-Lemus, B. González-Díaz, D. Borchert, Effect of porous silicon stain etched on large area alkaline textured crystalline silicon solar cells, *Thin Solid Films* (2009). https://doi.org/10.1016/j.tsf.2008.09.070

[32] R. A. Sinton, A. Cuevas, Contactless determination of current–voltage characteristics and minority-carrier lifetimes in semiconductors from quasi-steady-state photoconductance data, *Appl. Phys. Lett.* 69 (1996) 2510–2512.

[33] F. Montalvo-Galicia, M. T. Sanz-Pascual, P. Rosales-Quintero, M. Moreno-Moreno, Solar cell parameter extraction method from illumination and dark I–V characteristics, Nanomaterials 12 (2022) 1955. https://doi.org/10.3390/nano12121955

[34] D. Nobili, Precipitation as the phenomenon responsible for the electrically inactive phosphorus in silicon, *J. Appl. Phys.* **53** (1982) 1484–1491.

[35] K. Ali, S. A. Khan, M. Z. Mat Jafri, Spin-on doping (SOD) and diffusion temperature effect on recombinations/ideality factor for solar cell applications, *Chalcogenide Lett. 9* (2012) 457–463.

[36] E. Q. B. Macabebe, E. E. van Dyk, Parameter extraction from dark current–voltage characteristics of solar cells, *S. Afr. J. Sci.* 104 (2008) 401–404.

[37] A. Kaminski, J. J. Marchand, A. Laugier, Non ideal dark I–V curves behavior of silicon solar cells, *Sol. Energy Mater. Sol. Cells* **51** (1998) 221–231.

[38] A. S. H. van der Heide, A. Schönecker, J. H. Bultman, W. C. Sinke, Explanation of high solar cell diode factors by non-uniform contact resistance, *Prog. Photovolt. Res. Appl.* 13 (2005) 3–16.

[39] O. Breitenstein, P. Altermatt, K. Ramspeck, M. A. Green, J. Zhao, A. Schenk, Interpretation of the commonly observed I–V characteristics of c-Si cells having ideality factor larger than two, in: Conf. Rec. 2006 IEEE 4th World Conf. Photovoltaic Energy Conversion (WCPEC-4), Waikoloa, 2006, pp. 879–884. https://doi.org/10.1109/WCPEC.2006.279597

[40] A. Cuevas, D. Macdonald, Measuring and interpreting the lifetime of silicon wafers, *Sol. Energy* 76 (2004) 255–262.